

A&A manuscript no.  
(will be inserted by hand later)

Your thesaurus codes are:  
03 (11.01.2; 11.09.1; 11.17.2; 11.19.1; 13.25.2)

ASTRONOMY  
AND  
ASTROPHYSICS  
30.9.2018

# Soft X-ray properties of the Seyfert 1.8 galaxy NGC 3786

Stefanie Komossa, Henner Fink<sup>†</sup>

Max-Planck-Institut für extraterrestrische Physik, 85740 Garching, Germany

Received 3 February 1997; accepted June 1997

**Abstract.** An analysis of survey and pointed *ROSAT* PSPC observations of the Seyfert 1.8 galaxy NGC 3786 has revealed interesting spectral and temporal behaviour. The spectrum is found to show clear signs of excess absorption, and there is evidence that part (or all) of it is caused by the presence of a warm absorber. The soft X-ray spectral properties are discussed in the context of the Sy 1.8 classification of NGC 3786, and are combined with published optical data in an effort to discriminate between several possible absorption models. The one involving a warm absorber *with internal dust*, located between BLR and NLR, is favoured and shown to account successfully for the high observed broad line reddening as well as for the strong X-ray variability (a factor  $\sim 10$ ) we detect between the 1990 and 1992 observation.

**Key words:** Galaxies: active – individual: NGC 3786 – emission lines – Seyfert – X-rays: galaxies

## 1. Introduction

NGC 3786 (Mrk 744) is a spiral galaxy at a redshift of  $z=0.009$  that hosts an active nucleus. The galaxy forms a pair with its peculiar companion NGC 3788 and is included in several studies of Seyferts with companions (e.g. Keel et al. 1985, Keel 1996; Rafanelli et al. 1995).

The Seyfert nature of NGC 3786 was first noted by Afanas'ev et al. (1979a). Detailed optical spectroscopy was presented by Afanas'ev et al. (1979b) and by Goodrich & Osterbrock (1983; GO83 hereafter). GO83 classified the spectrum as Seyfert 1.8 according to the scheme of Osterbrock (1981). The galaxy is included in several investigations of the nature of Sy 1.8 and Sy 1.9 galaxies (e.g. Goodrich 1989, 1990; De Zotti & Gaskell 1985; Maiolino & Rieke 1995). One of the characteristics of the intermediate type Seyferts is steep Balmer decrements of the

broad lines (Osterbrock 1981). The cause for this is still under discussion, as is their place in the unified model of Seyfert galaxies (e.g. Lawrence 1987, Antonucci 1993). One interpretation is that intermediate type Seyferts are viewed through dusty material which causes the high observed Balmer line flux ratios by extinction, and which may be identified with an inner (e.g. Goodrich 1995) or outer (Maiolino & Rieke 1995) torus.

Recently, Nelson (1996) presented strong evidence for a thermal dust origin of the IR continuum of NGC 3786, through the analysis of a correlated, but time-delayed optical-IR outburst.

In X-rays, an upper limit for the count rate in the *HEAO 1* survey is reported by Persic et al. (1989). We are not aware of any more detailed X-ray study of NGC 3786. For the present investigation, we have analyzed the survey and archival pointed *ROSAT* (Trümper 1983) observations of NGC 3786 performed with the PSPC (Pfeffermann et al. 1987). Besides other soft X-ray properties, the amount of X-ray absorption present is particularly interesting in view of the Sy 1.8 character of NGC 3786, and *ROSAT* with its (0.1–2.4 keV) energy range is well suited for such a study.

The paper is organized as follows: In Sect. 2 we present the observations. The analysis of the data with respect to their spectral and temporal properties is described in Sects. 3 and 4, respectively. In Sect. 5, the X-ray spectrum is discussed in light of the Sy 1.8 classification of NGC 3786, and the inferences drawn from the X-ray data are combined with published optical observations. A summary and the conclusions are given in Sect. 6.

A distance of 54 Mpc is adopted for NGC 3786 assuming a Hubble constant of  $H_0 = 50$  km/s/Mpc and the galaxy to follow the Hubble flow. If not stated otherwise, cgs units are used throughout.

## 2. Data reduction

### 2.1. Pointed data

The observation was performed with the *ROSAT* PSPC on Dec. 6, 1992, with NGC 3786 in the centre of the field

Send offprint requests to: St. Komossa, skomossa@mpe-garching.mpg.de

<sup>†</sup> deceased in Dec. 1996

of view. The effective exposure time was 2.9 ksec. In total, 17 X-ray sources were detected with a likelihood  $\geq 10$  within the field of view. The positions of those sources in the vicinity of NGC 3786 are shown in Fig. 1, overlaid on an optical image from the digitized Palomar sky survey (E plate). The X-ray position of the pointlike central source is at  $\alpha = 11^{\text{h}}39^{\text{m}}42.7^{\text{s}}$ ,  $\delta = 31^{\circ}54'39.0''$  (J 2000), consistent with the optical position  $\alpha = 11^{\text{h}}39^{\text{m}}42.6^{\text{s}}$ ,  $\delta = 31^{\circ}54'33.4''$  (Clements 1983). The uncertainty in the X-ray position resulting from the telescope boresight error is of the order of  $10'' - 15''$  (Briel et al. 1994).

For further analysis, source photons were extracted within a circle centered around the X-ray position of NGC 3786. The background was determined from the inner  $19'$  of the field of view, after the removal of all detected sources. Vignetting and dead-time corrections were applied to the data using the EXSAS software package (Zimmermann et al. 1994). The mean source count rate is  $0.36 \pm 0.01$  cts/s. The other X-ray sources shown in Fig. 1 are weak, with count rates of about 0.01, 0.01, and 0.007 cts/s, respectively, ordered by increasing distance from the target source. For the spectral analysis source photons in the amplitude channels 11-240 were binned according to a constant signal/noise ratio of  $7\sigma$ . For the temporal analysis the minimal bin size in time was 400 s to account for the wobble mode of the observation.

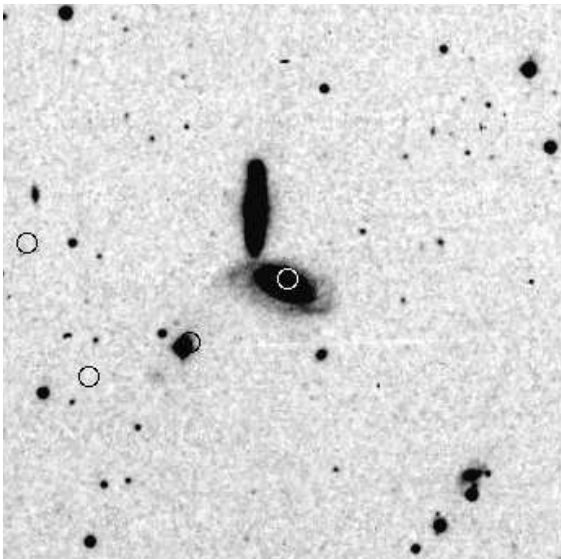


**Fig. 1.** X-ray sources detected in a  $10' \times 10'$  field around NGC 3786 superimposed on an optical image. The circles drawn around the X-ray source positions are of  $10''$  radius.

## 2.2. Survey data

The sky field around NGC 3786 was observed during the ROSAT all-sky survey (RASS) from Nov. 24 – 26, 1990,

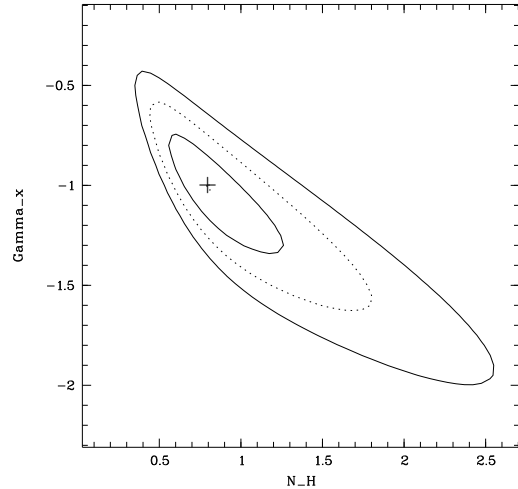


**Fig. 2.** Error ellipses in  $\Gamma_x$ ,  $N_{\text{H}}$  (in units of  $10^{21} \text{ cm}^{-2}$ ) for the single-powerlaw description of the X-ray spectrum. The two dimensional contours are shown for confidence levels of 68.3, 95.5 and 99.7%. The Galactic absorbing column density is  $N_{\text{H}} = 0.222 \times 10^{21} \text{ cm}^{-2}$ .

with an effective exposure time of about 400 s. Emission from NGC 3786 is detected, but found to be much weaker than in the pointed observation. After determining the background from a source-free region along the scanning direction of the telescope and correcting the data for vignetting, we find a source count rate of  $0.04 \pm 0.01$  cts/s. Due to the low number of detected photons no spectral analysis of the RASS observation can be performed and the following results (Sect. 3) refer to the pointed data only. The detected X-ray variability will be further discussed in Sect. 4.

## 3. Spectral analysis

### 3.1. Standard spectral models

A single powerlaw with cold absorption column as a free parameter acceptably fits the X-ray spectrum ( $\chi_{\text{red}}^2 = 1.0$ ), although some systematic residuals remain around 0.6–1.0 keV. The deduced power law is unusually flat, with a photon index  $\Gamma_x \simeq -1.0$ . An absorbing column of  $N_{\text{H}} \simeq 8 \times 10^{20} \text{ cm}^{-2}$  is found, exceeding the Galactic value towards NGC 3786 of  $N_{\text{H}} = 2.22 \times 10^{20} \text{ cm}^{-2}$  (Murphy et al. 1996). Fig. 2 displays the error ellipses for this model description.

Among various non-powerlaw spectral models compared to the data, including thermal bremsstrahlung, a Raymond-Smith model with cosmic abundances (Raymond & Smith 1977), and emission from an accretion disk after Shakura & Sunyaev (1973), only a black body gives an acceptable fit with  $kT_{\text{bb}} \simeq 0.5$  keV ( $\chi_{\text{red}}^2 = 1.2$ ). The cold column density is found to be consistent with the Galactic value in this case. Again, some systematic residuals remain around 0.6–1.0 keV.

The application of a powerlaw model with an additional absorption edge gives an excellent fit ( $\chi^2_{\text{red}} = 0.7$ ). We find an edge energy of  $E \approx 0.8$  keV and a photon index of  $\Gamma_x = -1.9 \pm 0.3$ . The cold absorption, with  $N_{\text{H}} = (1.7 \pm 0.3) \times 10^{21} \text{ cm}^{-2}$ , largely exceeds the Galactic value. The edge energy is near that expected for OVII ( $E = 0.74$  keV) and OVIII ( $E = 0.87$  keV). This is very suggestive of the presence of a warm absorber, which is discussed in more detail in the next section.

### 3.2. Warm absorber models

#### 3.2.1. Model properties and assumptions

To calculate the X-ray spectral absorption structure resulting from a warm absorber (WA) we used the photoionization code *Cloudy* (Ferland 1993). The warm material was assumed to be photoionized by the continuum emission of the nucleus, to be one-component and of constant density. Solar abundances (Grevesse & Anders 1989) were adopted. In those models that include dust mixed with the warm gas, the dust composition and grain size distribution were like those of the Galactic diffuse interstellar medium, and the chemical abundances depleted correspondingly, as in Ferland (1993).

The spectral energy distribution incident on the warm material was chosen to be a ‘mean Seyfert’ continuum. It consists of an UV-EUV powerlaw of energy index  $\alpha_{\text{UV-X}} = -1.4$  extending up to 0.1 keV, a mean optical to radio continuum after Padovani & Rafanelli (1988), a break at  $10 \mu\text{m}$  and an index  $\alpha = -2.5$   $\lambda$ -longwards. For comments on the usually weak influence of non-X-ray spectral parts on the warm absorption structure see Komossa & Fink (1997a).

Those two properties characterizing the warm absorber that can be directly extracted from X-ray spectral fitting are the hydrogen column density  $N_{\text{w}}$  of the ionized material and the ionization parameter  $U$ . The latter is defined as

$$U = Q / (4\pi r^2 n_{\text{H}} c) \quad (1)$$

where  $Q$  is the number rate of incident photons above 13.6 eV,  $r$  is the distance between nucleus and warm absorber,  $n_{\text{H}}$  is the hydrogen density (fixed to  $10^{9.5} \text{ cm}^{-3}$  unless noted otherwise) and  $c$  the speed of light.

#### 3.2.2. Model results

For the comparison of the warm absorber model with the X-ray spectrum of NGC 3786,  $\Gamma_x$  was fixed to  $-1.9$ , since we particularly wanted to test whether the data could be reconciled with a more typical Seyfert spectrum of canonical photon index. This value of  $\Gamma_x$  is also suggested by the single-edge fit to the spectrum. The value of the cold absorbing column is less certain, and may well exceed the Galactic value. In the following, we in turn discuss several

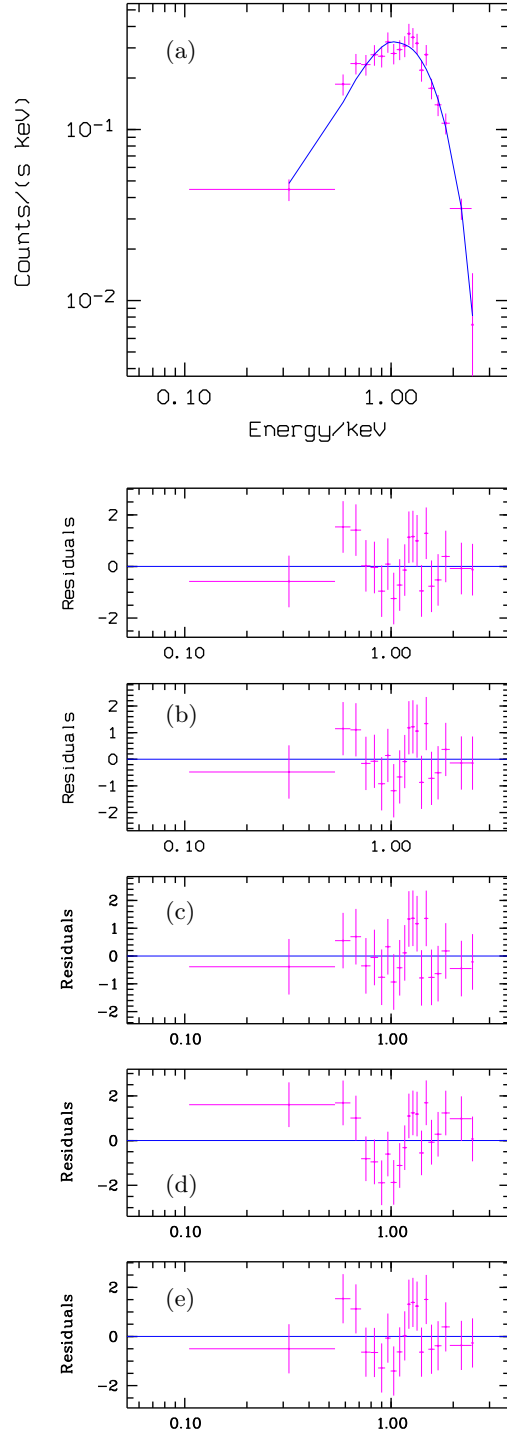


**Fig. 3.** The upper panel (a) shows the observed X-ray spectrum of NGC 3786 (crosses) and the best-fit dusty warm absorber model with fixed  $N_{\text{H}}$  (solid line; model 6 of Table 1). The second panel displays the fit residuals for this model. In the third panel (b) the residuals from the same model, but with  $N_{\text{H}}$  as additional free parameter (model 7), are depicted and in the fourth panel (c) those of the description involving a dust-free warm absorber (model 5). For comparison, the residuals resulting from a single powerlaw fit to the data are shown in the fifth panel (d). In all models so far, the powerlaw index was fixed to  $\Gamma_x = -1.9$ . The lowest panel (e) displays the residuals for the powerlaw fit with free photon index (model 1; note the slightly different scales in the ordinate).

**Table 1.** X-ray spectral fits to NGC 3786 (pl = powerlaw, bb = black body, wa = warm absorber). The errors are quoted at the 68% confidence level. The (0.1–2.4 keV) luminosity corrected for cold (and warm) absorption is  $L_x = (2.6, 1.9, 6.7) \times 10^{42}$  erg/s for models 1, 3, 4, respectively.

model	$N_H$ [ $10^{21} \text{ cm}^{-2}$ ]	$\log U$	$\log N_w$ [ $\text{cm}^{-2}$ ]	$\text{Norm}_{\text{pl}}^{(2)}$ [ $\text{ph}/\text{cm}^2/\text{s}/\text{keV}$ ]	$\Gamma_x$ or $kT_{\text{bb}}$ [keV]	$\text{Norm}_{\text{bb}}$ [ $\text{ph}/\text{cm}^2/\text{s}$ ]	$\chi^2(d.o.f)$
1 pl	$0.8 \pm 0.4$	-	-	$(2.0 \pm 0.7) 10^{-3}$	$-1.0 \pm 0.2$	-	16.4(17)
2a pl	$0.222^{(1)}$	-	-	$(1.5 \pm 0.1) 10^{-3}$	$-0.3 \pm 0.1$	-	45.0(18)
2b pl	$2.2 \pm 0.4$	-	-	$(3.1 \pm 0.3) 10^{-3}$	$-1.9^{(3)}$	-	26.7(18)
3 bb	$0.23 \pm 0.1$	-	-	-	$0.49 \pm 0.06$	$(3.4 \pm 0.3) 10^{-3}$	20.4(17)
4 wa	$0.222^{(1)}$	$-1.18 \pm 0.06$	$21.58 \pm 0.04$	$(5.0 \pm 0.4) 10^{-5}$	$-1.9^{(3)}$	-	14.3(17)
5 wa	$1.8 \pm 0.4$	$-0.31 \pm 0.22$	$21.78 \pm 0.16$	$(5.9 \pm 1.1) 10^{-5}$	$-1.9^{(3)}$	-	10.9(16)
6 dusty wa	$0.222^{(1)}$	$-0.81 \pm 0.04$	$21.71 \pm 0.02$	$(5.2 \pm 0.4) 10^{-5}$	$-1.9^{(3)}$	-	14.1(17)
7 dusty wa	$1.2 \pm 0.4$	$-0.30 \pm 0.25$	$21.74 \pm 0.23$	$(5.4 \pm 0.9) 10^{-5}$	$-1.9^{(3)}$	-	12.3(16)

<sup>(1)</sup> fixed to the Galactic value, <sup>(2)</sup> powerlaw flux, usually given at 1 keV, except for the models involving a warm absorber where it is given at 10 keV to represent the undistorted pl, <sup>(3)</sup> fixed

absorption models.

(i) *Dust-free WA.* In a first step, the value of the cold absorbing column was fixed to the Galactic value,  $N_H^{\text{gal}} = 2.22 \times 10^{20} \text{ cm}^{-2}$ . This model provides a very good fit ( $\chi_{\text{red}}^2 = 0.8$ ) with an ionization parameter of  $\log U \simeq -1.2$  and a column density of the ionized material of  $\log N_w \simeq 21.6$  (Table 1, model 4). The observed X-ray flux is  $f = 0.55 \times 10^{-11} \text{ erg}/\text{cm}^2/\text{s}$ , corresponding to an intrinsic (0.1–2.4 keV) luminosity corrected for cold and warm absorption of  $L_x = 6.7 \times 10^{42} \text{ erg}/\text{s}$ . Since the density of the warm material is essentially unconstrained by the X-ray spectral fits, only the density-scaled distance of the material from the nucleus is known. Assuming  $\log n_H = 9.5$  translates to a distance of  $r \simeq 0.016 \text{ pc}$  (using Eq. (1) and  $Q$  from integrating over the SED). The predicted warm-absorber intrinsic luminosity in  $H\beta$  is  $L_{H\beta} \simeq 2 \times 10^{40} \text{ erg}/\text{s}$ , assuming full covering.

Due to the possibility of partially compensating effects in the cold and warm column,  $N_H$  is not well constrained in the spectral fits. Nevertheless, in a second step, it was left as a free parameter. The best-fit column exceeds the Galactic value and a higher ionization parameter,  $\log U \simeq -0.3$ , is found for the warm absorber. Residuals around 0.6–1.0 keV are slightly better removed by this model than the previous one (Fig. 3c; Table 1, model 5).

(ii) *Dusty WA.* Finally, we also applied a dusty warm absorber model to the data. Warm material with internal dust was found to reproduce successfully the X-ray spectrum and other spectral properties of NGC 3227 (Komossa & Fink 1996, 1997b). Dusty warm gas was first suggested to exist in the infrared loud quasar IRAS 13349+2438 (Brandt et al. 1996). To account for the modification of the X-ray absorption structure due to the presence of dust

(Komossa & Fink 1997a,b), we re-calculated the warm absorber models, now including dust with Galactic ISM properties. Again, a successful fit is obtained. We find  $\log U \simeq -0.8$  and  $\log N_w \simeq 21.7$  for fixed cold Galactic column (Fig. 3a; Table 1, model 6), and  $\log U \simeq -0.3$ ,  $\log N_w \simeq 21.7$ ,  $N_H \simeq 1.2 \times 10^{21} \text{ cm}^{-2}$  for free cold column (Fig. 3b; Table 1, model 7).

A value of the gas density of  $\log n_H = 8$  was used to calculate the models that include dust, to ensure dust survival. The density-scaled distance of the warm material is given by  $r \simeq 0.055/\sqrt{n_8} \text{ pc}$ , where  $n_H = 10^8 n_8 \text{ cm}^{-3}$ . The emissivity of the gas in optical-UV emission lines is reduced as compared to the dust-free absorber.

Below (Sect. 5) we will try to select among the X-ray absorption models the one that accounts best for the observed properties of NGC 3786 in combining the X-ray spectral results with published multi-wavelength observations of NGC 3786 and constraints from X-ray variability (Sect. 4). For the sake of brevity, the different spectral models will occasionally be referred to by their number as given in Table 1.

#### 4. Temporal analysis

The X-ray lightcurve of NGC 3786 is shown in Fig. 4. Due to the wobble in the telescope’s pointing direction which causes a time dependent shadowing of the source’s image by the supporting grids, a reliable estimate of the source count rate is possible only by averaging the count rate over an entire wobble period of 400s. Since, usually, the total exposure time per satellite’s orbit is not an integer multiple of 400s, incomplete last bins were rejected in producing the X-ray lightcurve.

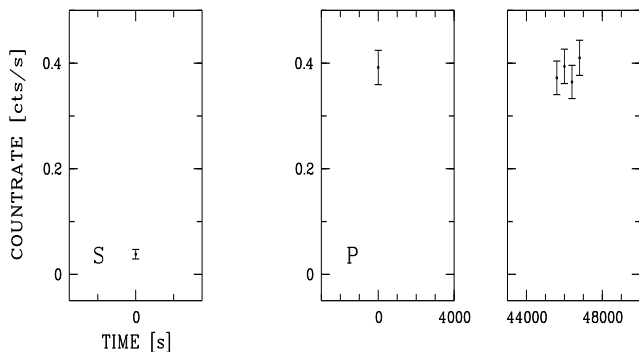


**Fig. 4.** X-ray lightcurve of NGC 3786, binned to time intervals of 400 s. The time is measured in seconds from the start of the observation; ‘S’ denotes survey, ‘P’ pointing.

The count rate during the pointed observation is constant within the errors. The source is found to be strongly variable on a longer timescale, however, since it is much weaker during the 2-year earlier *ROSAT* survey observation. The change in count rate (0.36 cts/s in the 1992 observation, 0.038 cts/s in 1990) is about a factor of 10.

## 5. Discussion

### 5.1. Comparison of different spectral models

Based purely on the quality of the X-ray spectral fits, three different models turn out to be successful: a black body, a flat powerlaw, and a warm-absorbed powerlaw of canonical spectral index. We favour the third one, since (besides hints for an absorption edge) the first two are very unusual as judged from previous X-ray observations of the class of Seyfert galaxies, and the presence of a dusty warm absorber also fits to other properties and observations of NGC 3786 (as detailed in Sect. 5.2).

Thermal emission (although not necessarily of blackbody-like shape) or a flat powerlaw may arise from a nuclear starburst, i.e. hot gas and/or supernova remnants and X-ray binaries. However, no other evidence of such a component is reported for NGC 3786, and the X-ray luminosity we find (a few  $10^{42}$  erg/s) overpredicts the one typically observed in galaxies with nuclear starbursts by a factor of  $\sim 10^3$  (e.g. Fabbiano 1989). Furthermore, such emission is not expected to vary by a factor of  $\sim 10$  within the timescale of 2 years. For a powerlaw emitted by the active nucleus, the one obtained (model 1) is *peculiarly flat*, with  $\Gamma_x = -1.0$ , as compared to the canonical value of  $-1.9$  (e.g. Pounds et al. 1994, Walter et al. 1994, Nandra et al. 1997).

The presence of a warm absorber removes the need for invoking such an unusually flat powerlaw, and strong evidence for ionized absorbers has been found in several of the well-studied Seyfert galaxies (cf. Fabian 1996 for a review). The amount of *cold* absorption present in NGC 3786 is more uncertain. A warm absorber model with Galactic

$N_H$  only already provides a successful fit. The warm material is found to be relatively lowly ionized in this case,  $\log U \simeq -1.2$  (still somewhat higher than is typical for the broad line region (BLR) itself), and also contributes to the low-energy absorption (Fig. 5). A successful alternative description is a more highly ionized absorber combined with excess cold absorption. The properties of the warm absorber are further discussed below in the context of the Sy 1.8 classification of NGC 3786.

### 5.2. Sy 1.8 nature of NGC 3786

#### 5.2.1. Spectral properties

An interesting characteristic of intermediate type Seyferts like NGC 3786 is the often rather steep Balmer decrement of the BLR as compared to Sy 1s. There are essentially two kinds of interpretations of the high observed  $H\alpha_b/H\beta_b$  flux ratio offered in the literature: One invokes reddening by dust along the line of sight, the other special properties of the BLR gas itself.

In the first scenario, the intrinsic flux ratio is near the case-B recombination (Brocklehurst 1971) value, and the observed deviations from that are caused by dust extinction (e.g. Osterbrock 1981). Some authors (e.g. Osterbrock 1981; Goodrich 1989, 1995) suggest the dust to be located in the outer BLR or just outside the BLR. This ensures dust survival, since dust is expected to be destroyed in the bulk of the BLR due to heating by the central radiation field and dust-gas interactions (e.g. Netzer 1990), and accounts for the usually less steep observed Balmer decrements of the NLR. Maiolino & Rieke (1995) propose the absorption to take place further outwards, in a 100 pc-scale torus (e.g. McLeod & Rieke 1995) coplanar with the galactic disk (their Fig. 6).

In the second interpretation (e.g. Canfield & Puetter 1981; Rudy et al. 1988), the flux ratio is *intrinsically* high. High values can be reached in a narrow range of optical depths and ionization parameters of the broad line gas (Canfield & Puetter 1981).

Evidence for the dust interpretation in some objects was presented by Goodrich (1989, 1995) based on line variability studies. In another approach, Goodrich (1990) distinguished between both scenarios based on the  $\text{Pa}\beta$  luminosity predicted in each case. For NGC 3786 he found no clear preference for either model.

In the present study, we find strong evidence for excess absorption along the line of sight to the X-ray continuum. However, due to the limited spectral resolution, the exact relative contributions of a warm and cold absorber cannot be clearly disentangled, and several models that provide a successful fit are interesting in the light of the Sy 1.8 character of NGC 3786: model 5 (Table 1) is reminiscent of the Maiolino&Rieke scenario, if we interpret the cold absorption to represent the outer torus, and the high- $U$  (dust-free) warm absorber the inner torus that is just grazed

along the l.o.s. On the other hand, in model 6 the dust mixed with the warm absorber would be located between BLR and NLR, more similar to the Goodrich scenario.

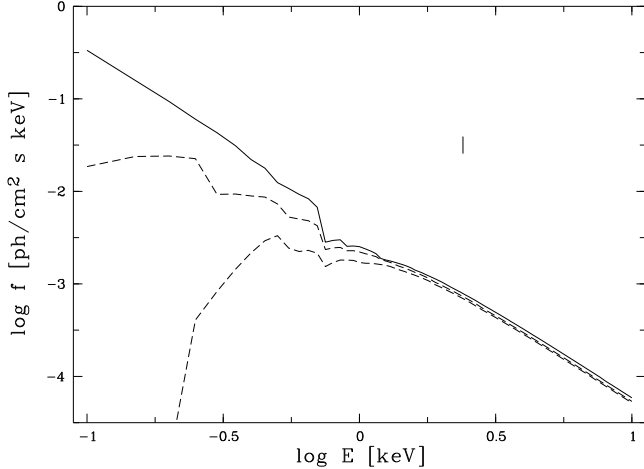


**Fig. 5.** Soft X-ray spectrum of NGC 3786 between 0.1 and 10 keV for several model descriptions. Solid line: dust-free warm absorber (model 5, Table 1); dashed lines: dusty warm absorber, upper dashed line: model 7, lower dashed line: model 6. All spectra plotted have been corrected for cold absorption. The vertical bar marks the upper end of the *ROSAT* energy range.

Given the different best-fit (warm or cold) absorbing columns we may ask which of the successful X-ray spectral models agrees best with the observed Balmer decrement. (We note that the optical and X-ray observations are not simultaneous, and time-dependent changes in the amount of reddening cannot be excluded; see also next section). GO83 derive a flux ratio of the broad Balmer lines of  $H\alpha_b/H\beta_b \simeq 8.4$ , which corresponds to an extinction of  $E_{B-V} \simeq 0.9$  (assuming an intrinsic flux ratio of 3.1 and a Galactic reddening law as in Osterbrock 1989). The narrow-line ratio,  $H\alpha_n/H\beta_n = 2.5$ , is near the case-B recombination value, indicating no reddening. Assuming that dust is indeed responsible for the steep Balmer decrement of the broad lines, and accompanied by an amount of cold gas as found in the Galaxy, we expect an absorbing column of  $N_H \simeq 5.5 \times 10^{21} \text{ cm}^{-2}$  (e.g. Bohlin et al. 1978; see also Predehl & Schmitt 1995). This is even larger than the value derived for the cold absorbing column in model 5 (Table 1). However, interestingly, it is very near the *warm* column  $N_w$  obtained for the fit of a dusty warm absorber. Ionized material with internal dust between NLR and BLR would therefore offer a nice explanation for the observed reddening properties.

The dusty gas is expected to further reveal its presence in the optical–UV spectral region: *If* the observed X-ray and UV continuum originate in a region of comparable extent as compared to that of the absorber, and travel along

the same paths, the optical–UV continuum will be altered by gas absorption lines and dust reddening. The equivalent widths of the UV absorption lines CIV  $\lambda 1549$  and NV  $\lambda 1240$  predicted to originate from the dusty warm absorber (model 6; the values for models 5,7,4, respectively, are given in brackets) are  $\log W_\lambda^{\text{CIV}}/\lambda \simeq -2.94$  ( $-3.06$ ,  $-3.01$ ,  $-2.90$ ) and  $\log W_\lambda^{\text{NV}}/\lambda \simeq -3.09$  ( $-3.13$ ,  $-3.09$ ,  $-2.98$ ; for a velocity parameter  $b = 60 \text{ km/s}$ , Spitzer 1978). A search for such features in high-quality UV spectra will certainly be worthwhile. The fraction of star light in the spectra of intermediate type Seyferts has been reported to be relatively high, which may indicate increased continuum reddening. For NGC 3786, the contribution is about 60% (GO83). However, we note that the optical spectral index of the non-stellar powerlaw is  $\alpha \simeq -1.0$  (GO83), which does not strongly deviate from the mean slope found for a sample of Seyfert 1s ( $\alpha \simeq -0.8$ ; Padovani & Rafanelli 1988).

The location of the dusty warm absorber is given by  $r \simeq 0.055 \text{ pc}/\sqrt{n_8}$  (Sect. 3.2.2). As noted in Sect. 1, Nelson (1996) found strong evidence for hot dust in the vicinity of the active nucleus of NGC 3786. He estimates an extent of the dust cloud of 0.033 to 0.062 pc from the nucleus. This component may be related to the warm absorber.

No BLR reverberation mapping results exist for NGC 3786. Assuming a scaling of BLR radius with luminosity as found in other objects (e.g. Netzer 1990, Peterson 1993) results in a smaller BLR radius in NGC 3786 than in NGC 3227. In the latter object, the bulk of the BLR emission was found to arise at about 0.01 pc (Salamanca et al. 1994, Winge et al. 1995). This value is consistent with a location of the warm absorber outside the BLR in NGC 3786.

As to the question whether the observed weak broad lines themselves may completely originate in the warm material (instead of a ‘usual’ BLR), we note that the absorber-intrinsic luminosity in  $H\beta$  is only  $\lesssim 1/40$  of the reddening-corrected observed broad  $L_{H\beta}$  (for model 4, in which it is strongest; and much weaker for the model involving dust mixed with the warm gas).

### 5.2.2. X-ray variability

A factor of  $\sim 10$  variability in count rate is detected between the 2-year-separated *ROSAT* observations. Pure *intrinsic* continuum variability is one possibility, another one is that we may have witnessed an event of increased absorption during the *ROSAT* survey observation due to either (a) changes in the cold (or warm) *column density*, or, (b) a reaction of the *ionization state* of the warm absorber to (small) changes in the intrinsic luminosity.

Events of changing emission-line extinction, on the timescale of years, have been reported by Goodrich (1989, 1995) for some intermediate Seyferts. The present observation may represent a similar event seen in X-rays.

In a series of simulations we have determined the required change in (a<sub>1</sub>)  $N_H$ , or (a<sub>2</sub>)  $N_w$ , or (b)  $L \Rightarrow U$  to

account for the observed drop in count rate. First of all, we note that due to the relative ‘hardness’ of the X-ray spectrum, comparatively high absorption will be required to change the count rate by a factor of 10 (since cold absorption mainly affects the low-E region, which already only weakly contributes to the total count rate during the pointed observation.) The high expected columns are not unusual for BLR clouds or warm absorbers, though. More specifically, we find (numerical values are representatively given for models 6 and 7 of Table 1):

(a<sub>1</sub>) A factor of 16 change in the cold column density is necessary to account for the low count rate of the survey observation, i.e.  $N_{\text{H}} \simeq 1.9 \times 10^{22} \text{ cm}^{-2}$  (model 7).

(b) In order to change sufficiently the absorption of the warm material by its response to a decrease in incident luminosity, we have to vary  $L$  by a factor of  $\sim 5$  (model 7). We consider this too large a factor to represent still an ‘elegant’ solution (in the sense that one may then as well contribute all observed variability to changes in intrinsic luminosity).

(a<sub>2</sub>) Finally, we varied  $N_{\text{w}}$ . Since the warm material more effectively absorbs at higher energies within the *ROSAT* band than a cold absorber, we expect a smaller change in  $N_{\text{w}}$  to be required as compared to  $N_{\text{H}}$ . A value of  $\log N_{\text{w}} \simeq 22.45$  (model 6; corresponding to a factor of  $\sim 5$  increase) reproduces the observed count rate.

Based on these findings we, again, favour the interpretation invoking the *dusty warm* absorber (model 6) which does not require additional cold absorption in excess of the Galactic value, i.e. accounts for all observations with the lowest number of components/parameters. In this model, then, a cloud of warm material may pass the line of sight with a larger column along the l.o.s. during the survey observation. (Of course, a dust-free BLR cloud in motion (and constant properties of the dusty WA; model 7) would have had the same effect on the X-ray spectrum, although requiring a stronger change in  $N_{\text{H}}$ . Both models differ in the optical emission line reddening they predict. The reddening should change in case of variable  $N_{\text{w}}$ , but be unaffected in case of variable dust-free cold  $N_{\text{H}}$ . Optical spectra taken simultaneously with the *ROSAT* observations would be valuable to discriminate between both possibilities.)

Concerning observations with previous X-ray satellites, Persic et al. (1989) report an upper limit for the count rate in the direction of NGC 3786 obtained during the *HEAO 1* survey of  $R15 < 0.86$  (with an error of 0.29), which converts to a luminosity of  $L < 6.6 \times 10^{42} \text{ erg/s}$  in the energy range 2–10 keV. We predict (2–10 keV) luminosities of  $L_1 = 8.7 \times 10^{42} \text{ erg/s}$  and  $L_{4-7} \simeq 4 \times 10^{42} \text{ erg/s}$  for models 1 and 4–7 of Table 1, respectively. This is consistent with the upper limit of Persic et al. (1989) within the errors, i.e. with an intrinsically constant continuum.

## 6. Summary and conclusions

We have reported the detection in X-rays of the Seyfert 1.8 galaxy NGC 3786. An analysis of the soft X-ray properties on the basis of *ROSAT* PSPC observations was performed. The two most conspicuous features are (i) evidence for strong excess absorption along the line of sight, part (or all) of which may be caused by the presence of a warm absorber, and (ii) high-amplitude variability between the 2y-separated observations of a factor of  $\sim 10$  in count rate, with an intrinsic (0.1–2.4 keV) luminosity of  $L_{\text{x}} \simeq$  a few  $\times 10^{42} \text{ erg/s}$  during the high-state.

These findings are discussed in the light of the Sy 1.8 nature of NGC 3786. From several absorption models that provide a successful description of the X-ray spectrum, we tentatively favour the one involving a warm absorber *with internal dust*, for which we obtain an ionization parameter of  $\log U \simeq -0.8$ , a column density of  $\log N_{\text{w}} \simeq 21.7$ , a density-scaled distance from the nucleus of  $r \simeq 0.055/\sqrt{n_{\text{s}}}$  pc, and a density  $n_{\text{H}} \lesssim 10^8 \text{ cm}^{-3}$ . Placing the dusty material between BLR and NLR, this model is shown to provide an explanation for (a) the observed steepness of the broad Balmer decrement (GO83) by dust reddening, and (b) the detected drop in the X-ray count rate by variability in the column density, e.g. by a cloud that crosses the line of sight. The warm absorber may be related to the dusty torus and/or the component of hot dust in NGC 3786 for which evidence was recently reported.

NGC 3786 certainly is a very interesting object for further X-ray spectral studies, particularly in combination with UV absorption line and optical reddening measurements.

*Acknowledgements.* We thank Gary Ferland for providing *Cloudy*, and Hartmut Schulz for a critical reading of the manuscript. The *ROSAT* project is supported by the German Bundesministerium für Bildung, Wissenschaft, Forschung und Technologie (BMBF/DARA) and the Max-Planck-Society. This research has made use of the NASA/IPAC extragalactic database (NED) which is operated by the Jet Propulsion Laboratory, Caltech, under contract with the National Aeronautics and Space Administration. The optical image shown is based on photographic data of the National Geographic Society – Palomar Observatory Sky Survey (NGS-POSS) obtained using the Oschin Telescope on Palomar Mountain. The NGS-POSS was funded by a grant from the National Geographic Society to the California Institute of Technology. The plates were processed into the present compressed digital form with their permission. The Digitized Sky Survey was produced at the Space Telescope Science Institute under US Government grant NAG W-2166.

## References

- Afanas’ev V.L., Denisjuk E.K., Lipovetskii V.A., 1979a, PisAZ 5, 271
- Afanas’ev V.L., Lipovetskii V.A., Shapovalova A.I., 1979b, Afz 15, 557
- Antonucci R., 1993, ARA&A 31, 473

- Bohlin R.C., Savage B.D., Drake J.F., 1978, ApJ 224, 132
- Brandt W.N., Fabian, A.C., Pounds K.A., 1996, MNRAS 278, 326
- Briel H., Aschenbach B., Hasinger G., et al., 1994, *ROSAT user's handbook*
- Brocklehurst M., 1971, MNRAS 153, 471
- Canfield R.C., Puetter R.C., 1981, ApJ 243, 390
- Clements E.D., 1983, MNRAS 204, 811
- De Zotti G., Gaskell C.M., 1985, A&A 147, 1
- Fabbiano G., 1989, ARA&A 27, 87
- Fabian A.C., 1996, MPE Report 263, H.U. Zimmermann, J. Trümper, H. Yorke (eds.), 403
- Ferland G.J., 1993, University of Kentucky, Physics Department, Internal Report
- Goodrich R.W., 1989, ApJ 340, 190
- Goodrich R.W., 1990, ApJ 355, 88
- Goodrich R.W., 1995, ApJ 440, 141
- Goodrich R.W., Osterbrock D.E., 1983, ApJ 269, 416 (GO83)
- Grevesse N., Anders E., 1989, in *Cosmic Abundances of Matter*, AIP 183, C.J. Waddington (ed.), New York: American Institute of Physics
- Keel W.C., 1996, AJ 111, 696
- Keel W.C., Kennicutt R.C., Hummel E., Van der Hulst J.M., 1985, AJ 90, 708
- Komossa S., Fink H., 1996, AG Abstract Series 12, 228
- Komossa S., Fink H., 1997a, A&A 322, 719
- Komossa S., Fink H., 1997b, A&A, in press
- Lawrence A., 1987, PASP 99, 309
- Maiolino R., Rieke G.H., 1995, ApJ 454, 95
- McLeod K.K., Rieke G.H., 1995, ApJ 441, 96
- Murphy E.M., Lockman F.J., Laor A., Elvis M., 1996, ApJS 105, 369
- Nandra K., George I.M., Mushotzky R.F., Turner T.J., Yaqoob T., 1997, astro-ph/9606169, to appear in ApJ
- Nelson B.O., 1996, ApJ 465, L87
- Netzer H., 1990, in Saas-Fee Lecture Notes 20, T.J.-L. Courvoisier and M. Mayor (eds.)
- Osterbrock D.E., 1981, ApJ 249, 462
- Osterbrock D.E., 1989, *Astrophysics of Gaseous Nebulae and Active Galactic Nuclei*, Univ. Sci. Books: Mill Valley
- Padovani P., Rafanelli P., 1988, A&A 205, 53
- Persic M., De Zotti G., Danese L., et al., 1989, ApJ 344, 125
- Peterson B., 1993, PASP 685, 247
- Pfeffermann E., Briel U.G., Hippmann H., et al., 1987, SPIE 733, 519
- Pounds K.A., Nandra K., Fink H., Makino F., 1994, MNRAS 267, 193
- Predehl P., Schmitt J.H.M.M., 1995, A&A 293, 889
- Rafanelli P., Violato M., Baruffolo A., 1995, AJ 109, 1546
- Raymond J.C., Smith B.W., 1977, ApJS 35, 419
- Rudy R.J., Cohen R.D., Ake T.B., 1988, ApJ 332, 172
- Salamanca I., Alloin D., Baribaud T., et al., 1994, A&A 282, 742
- Shakura N.I., Sunyaev R.A., 1973, A&A 24, 337
- Spitzer L., 1978, *Physical Processes in the Interstellar Medium*, Wiley: New York
- Trümper J., 1983, Adv. Space Res. 2, 241
- Walter R., Orr A., Courvoisier T.J.-L., et al., 1994, A&A 285, 119
- Winge C., Peterson B., Horne K., et al., 1995, ApJ 445, 680
- Zimmermann H.U., Becker W., Belloni T., et al., 1994, MPE report 257